PREROTATION AND FLUID RECIRCULATION IN THE SUCTION PIPE OF CONTRIFUGAL PUMPS

by

F.A.E. Breugelmans

Professor and Head, Turbomachinery Department

von Karman Institute for Fluid Dynamics

Saint Genése, Belgium

and

M. Sen

Assistant Professor, Istanbul Technical University

Istanbul, Turkey

Professor F. A. E. Breugelmans studied Mechanical Engineering at the University of Leuven, Belgium. He did postgraduate work in fluid dynamics at the von Karman Institute for Fluid Dynamics, where he later joined as a research assistant in 1964.

From 1977 to the present, Professor Breugelmans has been the Head of the Turbomachinery Department at the von Karman Institute, where he has been teaching, consulting and conducting research in axial flow compressors.

He has also been a visiting Assistant Professor at Iowa State and currently holds ASME, AGARD-PEP, ISABE membership.

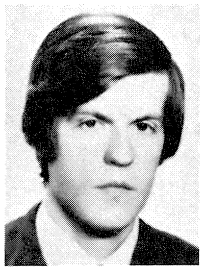

Dr. M. Sen received his Master of Science in Mechanical Engineering from the Technical University of Istanbul in 1970, where he is presently an Assistant Professor. He did Post-Graduate work in fluid dynamics at the von Karman Institute in Belgium, where he collaborated with Worthington Nord S.P.A. (Italy) on the paper entitled, "Inlet Flow Field of Centrifugal Pumps at Partial Deliveries."

After winning the H. Worthington European Technical Award in 1979, Dr. Sen earned his Ph.D. degree from the Universite Libre de Bruxelles in 1980.

ABSTRACT

Two groups of pumps were investigated in great detail and the analysis showed that large variations in Q_{CR}, for the same design specific speed, can be obtained by modifying the design of the rotating channels.

An attempt was made to condense the different design parameters into a global parameter, relating the design concept and the critical flow rate, for analysis and prediction purposes.

INTRODUCTION

Centrifugal pumps are widely used in the fields of water supply, irrigation, pipelines, paper and petro-chemical industries, nuclear and steam power plants. These applications require a large operating range of the pumps as was shown in [1] and [2].

The performance characteristic of a hydraulic machine can in general be presented by a curve, traversing different quadrants in a ($\pm$ H, $\pm$Q) plane. A schematic representation is shown in Figure 1 where the constant speedlines N = $+N_1$, $-N_1$ and 0 are shown as well as the zero torque and the $+N_1$ torque curve. When a centrifugal pump operates at partial flow rates (a condition between the best efficiency point and shut-off) the flow in the suction pipe starts prerotating with the impeller and finally a reverse flow from the impeller towards the suction occurs at the outer periphery.

Prerotation and reverse flow have become evident by the abnormal suction pipe wall static pressure rise, the noise and vibration level, erosion of the blades and stationary parts. These symptoms and diagnosis are discussed in [1]. The energy losses caused by the reverse flow have an importance for the manometric head and shaft power of the pump. The fluctuating pressure and velocities have a direct impact on the mechanical damage. An extension of the reverse-free operating range of a centrifugal pump is, therefore, of great importance.

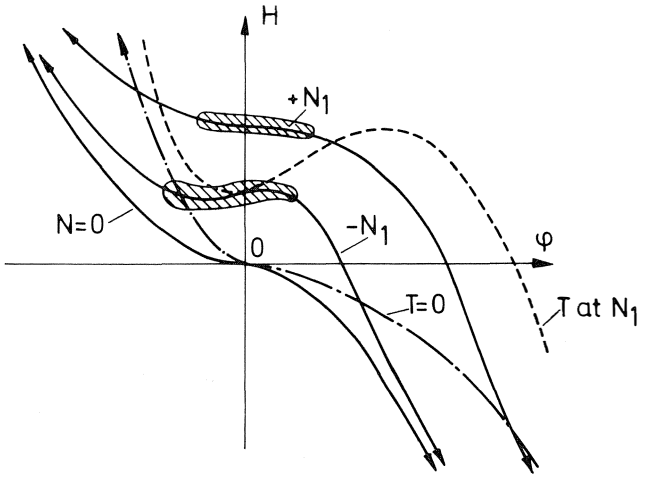

Figure 1. Characteristics of a Hydraulic Machine.

The unsteady flow phenomena in a pump can be classified into three categories:

- Small scale instabilities, such as the blade wakes and blade-to-blade fluctuating field, essential in the energy transfer between the mechanical parts and the fluid.
- The medium scale instabilities, such as prerotation, where more than one blade is involved, or rotating stall in a compressor.
- The large scale perturbations, such as surging of the total system. The variations and/or sign reversals of the flow rate are observed on an overall system's point of view.

All of these types are involved in some kind of recirculating flow, some of which are not observable outside the impeller.

This contribution focuses on the second type and the influence of design parameters upon the appearance of prerotation and reverse flow in the suction.

FLOW RECIRCULATION — PREROTATION

For high enough flow rates the flow in the straight part of the suction pipe is one dimensional, except of course in the wall boundary layer, and swirl free ($\alpha = 0$). These conditions satisfy the impeller design assumption where the flow entering the impeller is considered as axial.

The reduction of the flow rate by closing the throttle valve imposes a higher loading on the rotating impeller. Consider two streamlines; one following the outer radius of the inlet pipe and the impeller shroud, the second one following the inner radius along the hub contour. The inner streamline has a larger energy capability due to the larger radial shift that is experienced by the fluid following this trajectory. At an excessive loading for the outer streamline, the inner one still has the possibility to overcome the imposed pressure rise and a small amount of recirculation starts inside the rotating channels. The phenomenon is also controlled by the combined curvature in the meridional and blade-to-blade plane.

Let us consider a given axial station in the suction pipe and continue to reduce further the flow rate. When the flow rate is reduced a certain amount, the flow suddenly becomes three-dimensional at this section. That flow has negative axial velocity component at the outer part of the pipe (reverse flow) and flow is forward in the inner part of the pipe. The considered flow has an overall swirling character where the tangential component has its maximum value near the wall and decreases regularly towards the rotation axis. This swirling flow has the same direction of rotation as the impeller, hence named as "Prerotation". A general picture of the reverse flow and prerotation is illustrated in Figure 2. The radial component of the velocity is much smaller in value as compared to the axial and tangential components.

The flow rate for which reverse flow starts is named "Critical Flow Rate" for the considered section. Reverse flow propagates upstream and increases its intensity if the flow rate is further reduced and reaches its maximum at shut-off. The flow rate for which the reverse flow starts at the tip of the blade leading edge will be named "Pump Critical Flow Rate". This is the main parameter to be identified for the present study. Reverse flow and prerotation cause a change of the impeller inlet velocity triangles as shown in Figure 2.

Studies on this problem have started in the early 1900's. Stewart detected the prerotation with a special rotometer. Stepanoff [6] explained the occurrence of the prerotation with his "Least Resistance Principle" which assumes that the fluid

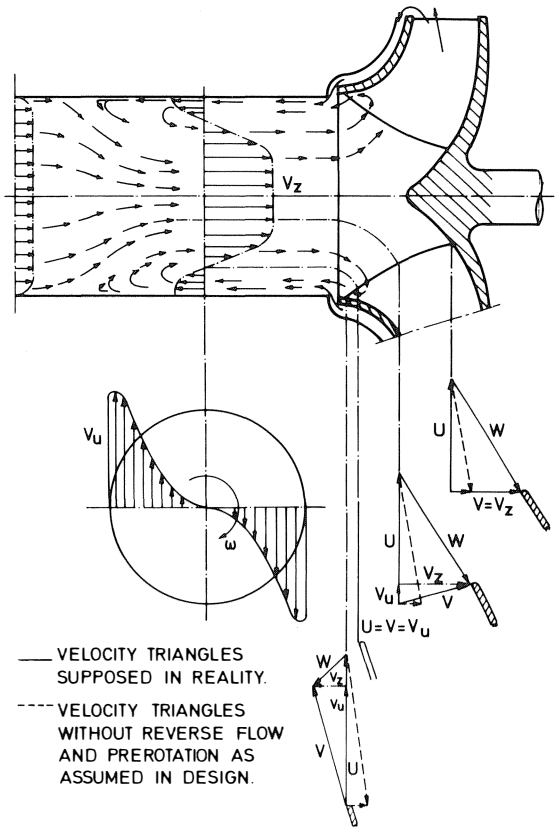

Figure 2. Prerotation and Preswirl.

follows a path in such a way to encounter the minimum resistance to enter the impeller. Hence, the fluid should acquire a tangential velocity component having the same sense as impeller rotation, at flow rates smaller than the nominal one in order to enter the impeller channel with an angle equal to the blade angle. An opposite tangential velocity component (contra-rotation) is required for the flow rates higher than the nominal one. But, such a contra-rotation has never been reported and observed. Our investigation indicated this existence between nominal and critical flow rate. In this flow pattern, no energy is transferred from the impeller to the fluid in the suction pipe. This hypothesis cannot be considered since the reverse flow is started by the impeller and all the energy of the reverse flow and prerotation is transferred from the impeller as is known from more recent data.

Benson and Moses tested a high speed, three-dimensional, unshrouded, straight radial bladed compressor and showed that the flow rate is the determining factor of the reverse flow characteristics. Reynolds number effects are negligible. The reverse flow resulted in a high degree of turbulence in the inlet pipe at the impeller entrance. For this case, the axial velocity component did not appreciably change with flow rate and the degree of prerotation was insignificant near the center of the suction pipe.

Peck [7] tested an unshrouded centrifugal pump impeller matched with a volute. He showed that the inlet flow angle becomes very unsteady at the critical flow rate of the test section where the measurements are performed. The inlet flow becomes asymmetric when the reverse flow appears. He attributed the inlet flow asymmetry to the asymmetric pressure distribution around the volute and explained the gradual decay

of the swirling reverse flow by the friction between the pipe wall and liquid.

Schweiger [8] observed the variation of the reverse flow intensity as a function of the pump geometrical parameters; such as number of blades, impeller inlet diameter, volute ring diameter. The measurements were only performed at shut-off and using air as the fluid. These test impellers are of low specific speed, two-dimensional, shrouded, straight radial blades. The volute was made cylindrical with parallel side walls, i.e., axisymmetric. He observed a dead space in the core of the pipe where there was no indication of flow at all. At the outside of the core, the velocity field rotated impellerwise with indication of a strong forced vortex. The size of the dead zone was gradually increased with increase of the suction pipe diameter. The core ratio (core diameter/suction pipe diameter) approaches an asymptotic value and reaches its maximum at impeller ratio (D_1/D_2) of 0.6. The influence of the blade number and volute ring diameter on the size of the core is negligible. The continuity was satisfied by finding that the flow rates of the forward and reverse flows were equal and no inlet asymmetry was noticed.

Murakami and Heya [9] investigated a diagonal flow type shrouded pump impeller. Pump critical flow rate was found at $Q_{cr}/Q_N = 0.86$. At flow rates smaller than the critical flow rate, the velocity distribution exhibited a close resemblance to the profile of a forced vortex motion, except in the wall region. The maximum value of the radial component of the velocity is in order or magnitude of 1/10 of the other components. Swirling reverse flow showed similar profiles of velocity distributions with different pump speeds. It was concluded that the variation of the velocity with the pump rotational speed follows the law of simila ity as reported by Schiavello [4]. The symmetry of the flow was checked by measuring the velocity along two orthogonal diameters of the suction pipe, at different sections. The results indicated no significant eccentricity. The flow rate evaluated by graphical integration of the axial velocity component and by a volumetric method showed an important discrepancy at very low flow rates. He considered the strength of the swirling flow to be largely controlled by the contour of the blade leading edge, especially by the ratio of $R_{1,H}/R_0$. To show this, he carried out experiments on a mixed flow pump and on a radial flow pump. By reducing the flow rate, the reverse flow extended progressively farther from the pump inlet and reached up to 7 pipe diameters distance at shut-off. It was shown that the velocity field may be considered as axisymmetric but the wall pressure angular distributions showed a considerable asymmetry. The average value of the wall pressure distribution was affected by the piping installation. Reverse flow did not penetrate a 90° elbow. Some of the reverse flow passed through a 45° elbow, resulting in a complex flow upstream of the elbow.

Murakami and Heya [9] presented a theory on the decay of a turbulent swirling flow in the suction pipe of centrifugal pumps. They assumed that swirling flow is of the forced vortex type and that it decays in the upstream direction maintaining the same profile. Assumed simplified velocity component distributions were based on the experimental results of a diagonal type pump impeller. The flow field was given in empirical formulas in function of only flow rate for a given section, independent of the pump.

The research work of Ferrini [3], Schiavello [4] and Sen [5] examined the blade number and volute effects experimentally. Test impellers differed only in the blade number, keeping the same meridional channel and blade profiles. Three impellers were matched with two different designs of the volute. One was of the free vortex type and the other one was designed assuming the mean velocity is constant around the volute. Critical flow rates of four tested configurations were close to each other, within the range of $Q_{cr}/Q_N = 0.55 \leftrightarrow 0.62$, at the test section of $x/R_0 = 0.4$. The velocity and energy radial distributions showed similar profiles in shape and value. Flow traverses made along two orthogonal diameters showed remarkable inlet asymmetry. The flow was reversed at the outer circumference, occupying 40% of the total area. Inlet wall pressure circumferential distributions showed a significant dependency on the configuration.

Mizuki examined the reverse flow phenomena in a centrifugal compressor. The compressor consisted of a shrouded inducer, unshrouded impeller, vaneless diffuser and volute. At 50% of the nominal flow rate, reverse flow took place at the inlet of the inducer while no apparent reversed flow was observed within the inducer and impeller. But, there was evidence of the forming of low velocity zones and eddies in the impeller. The turbulence intensity of the inlet flow increased just at the start of the flow reversal and then decreased with decreasing flow rate. The oil streak on the outer wall within the inlet duct showed a time averaged reverse flow, also.

Many of the authors have performed pump tests in air at sufficiently high Reynolds Numbers ($> 5 \times 10^5$) and studied stall in centrifugal compressors in order to shed some light on the prerotation phenomenon.

The conclusions of the different researchers are sometimes contradictory, especially concerning the asymmetry and the dependence of prerotation upon geometrical configurations.

METHODS TO DELAY PREROTATION — STABILITY

Stability of the pump total head is defined as the increase of manometric head with a decrease of flow rate (negative head gradient). Since the reverse flow causes some amount of energy losses at partial flow rates, instability was often attributed directly to the occurrence of the reverse flow and prerotation. Therefore, some devices were studied in order to improve the head stability, but at the expense of the performances at nominal and high flow rates and mostly caused a shift of the best efficiency point.

Lewthwaite and Worster [10] reported that it does not seem possible to alter the shut-off head and the stability of the head by inlet guide vanes which leave the best efficiency point unchanged. None of the inlet guide vane arrangements which were tested on a centrifugal pump operating with air, improved the unstable head (Figure 3). Only one configuration increased the head while the shaft power increased. Schmeidl [11] found an opposite trend to the results obtained by Lewthwaite and Worster [10]. He tested diagonal type shrouded pump impellers which had an unstable head, with different inlet flow straighteners, and all of them made the pump characteristic stable with an increase of shaft power as shown in Figure 4.

Murakami and Heya improved a head performance of a high specific speed diagonal type pump at low flow rates by throttling the impeller eye. An increase of head and a decrease of shaft power was observed while the reverse flow losses decreased. The saving in power caused by this throttling was approximately equal to the power loss due to the reverse flow under conventional operation (without throttling). But, pump performance was spoiled drastically when the pump operated at high flow rates.

Dufays [12] throttled the impeller eye in two different ways, keeping the net inflow area constant for both configura-

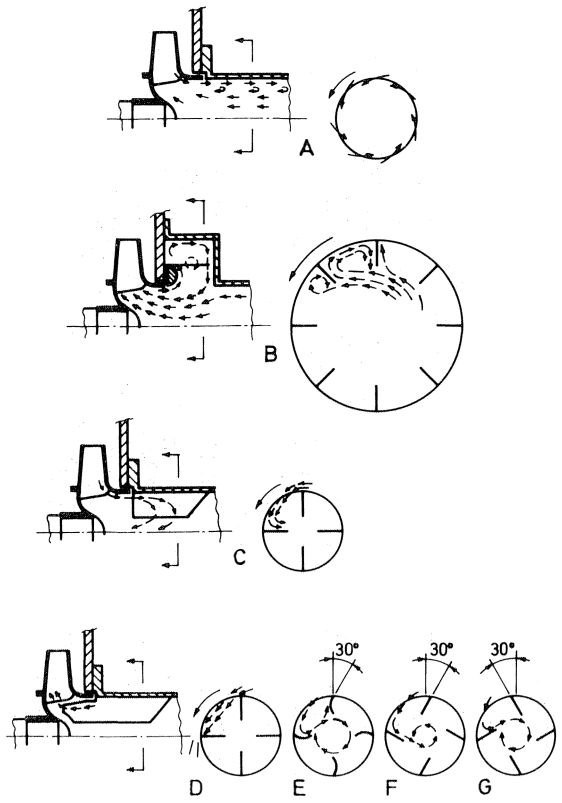

Figure 3. Inlet Guide Vane Systems — Centrifugal Pump [10].

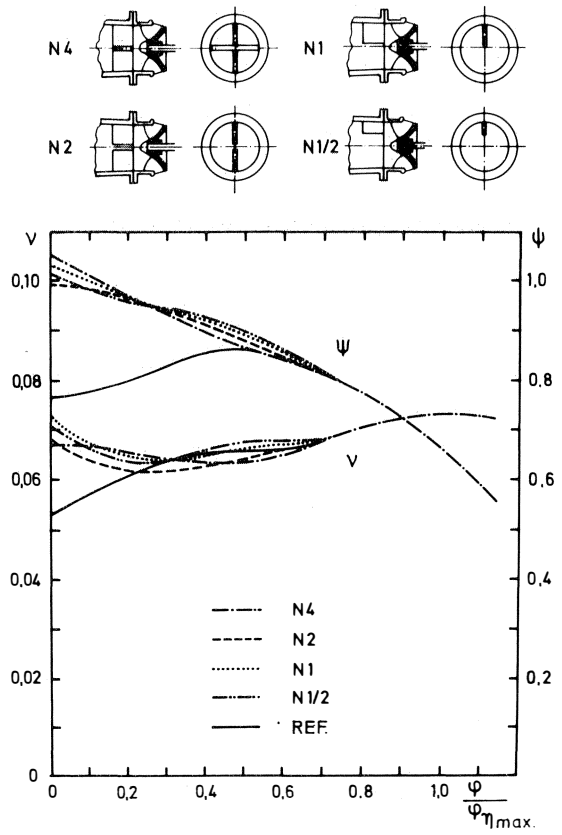

Figure 4. Inlet Guide Vane Systems — Mixed Flow Pump [11].

tions. One was throttling by a diaphram and the other one was by using a disc attached to the impeller shaft. The critical flow rate and reverse flow losses were reduced slightly for both configurations, but a reduction of the head and efficiency occurred at normal flow rates, as shown in Figure 5. Wall static pressure circumferential distributions at the upstream of the throttling devices showed the same type of asymmetry for both configurations, but decreased in value for the diaphram case.

Worster [13] modified the inlet, that was found to raise the shut-off head, to reduce the shaft power. This was done to make the performance stable. The impeller eye was blanked off from the inlet pipe with a disc attached to the impeller and rotating with it. A similar but stationary disc had no effect on the performance. It was concluded that the flow at the impeller inlet influences the stability in much the same way as the outlet; the low head at shut-off is caused by excessive recirculation due to radial unbalance in the inlet and due to circumferential unbalance in the outlet.

Schweiger [14], studied the impeller leading edge position and inlet straightener influence on the low specific speed pump stability. The first idea was that the recirculatory flow in the suction pipe is reduced by inlet straighteners and by extending the blades into the suction eye of the impeller. The best stability was found if the leading edge is perpendicular to the rotation axis (Figure 6). The effect was stronger with double curvature blades than with the single curvature blades. A similar effect was obtained with straighteners and reduced suction pipe diameter. In fact, the centrifugal pump head stability is primarily affected by the volute design, position and shape of the volute tongue, vaned diffusers, impeller-volute matching, and the area ratio of volute throat to impeller eye reported by the different researchers.

The purpose of this research was to perform a systematic investigation and study how in the design phase the occurrence of prerotation can be delayed and how for given designs the critical flow rate can be predicted.

FACILITY DESCRIPTION

The experiments of this systematic study were carried out in the VKI P-2 pump facility. The pump test rig operates as a closed loop and uses water.

The facility is driven by a 180 kW DC motor with a maximum rpm of 3000 or 15000 with a step-up gear-box. The axis of the cylindrical settling chamber and the pump axis of

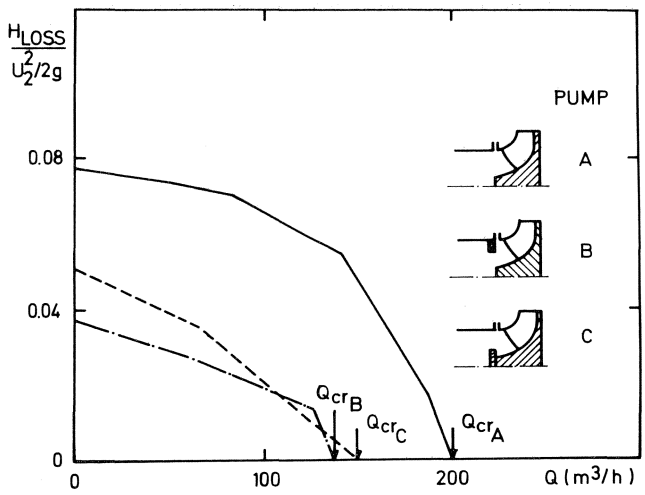

Figure 5. Inlet Throttling of a Centrifugal Pump [5].

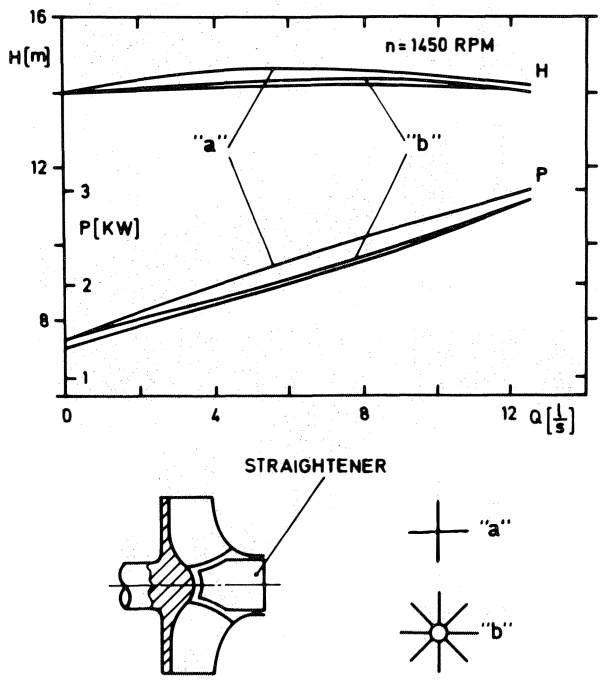

Figure 6. Inlet Straighteners [14].

rotation lie in a horizontal plane. A vacuum pump is connected to the settling chamber in order to deaerate the water and to depressurize the circuit for NPSH tests. A honeycomb is placed at the exit of the settling chamber and leads to a convergent duct and the pump suction pipe. The discharge is vertical and connects to a flow meter of the venturi type in the return branch of the loop. A heat exchanger in the by-pass circuit keeps the circulating water at constant temperature during the experiments, while the flow rate is controlled by two butterfly valves, one in the main discharge pipe and one in the by-pass.

The test rig accommodates centrifugal, mixed flow and inducer type of pumps with single or double volute and allows experiments over the full speed range.

The instrumentation allows global measurements to be taken of power, mass flow, total head, torque and also the detailed flow measurements using total, static pressure tappings, wedge type and cobra directional probes, pressure pick-ups and small rotating vanes for unsteady flow observation. The facility is shown in Figure 7.

INSTRUMENTATION

Overall measurements

The volumetric flow rate is measured by means of a standard AFNOR venturi, which was calibrated with a pitot probe in the same conditions as the testing. Static pressure differences across the venturi were measured by a U-tube differential mercury manometer.

The manometric head of the pump is measured as the total head difference between discharge section D and suction section S. Four holes around the circumference of the measurement sections S and D measure the mean average static pressures. The suction head measurement section is selected far enough from the pump inlet to avoid high static pressure readings due to the prerotation at partial flow rates. The suction and discharge static pressure difference is measured

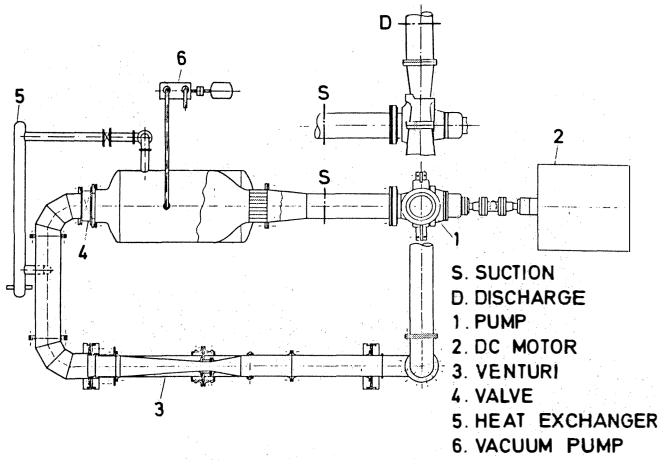

Figure 7. P-2 Test Facility.

with a differential type variable reluctance pressure transducer which has a high natural frequency, very stable and linear calibration characteristic. The kinetic energy difference due to the different diameters at the test sections is taken into account to determine the pump's manometric head.

The torque is measured by a strain gauge balance mounted on the free floating cage electrical motor. The torque-meter is calibrated statically.

The rotational speed is measured with a slotted disc fixed on the shaft and a photoelectric cell. A digital pulse counter provides the rotational speed readings with equal time intervals of four seconds. Pressure transducers and torque-meter reading are displayed on digital voltmeters.

Inlet flow surveys

A shaft, longer than the conventional and commonly used one, is fitted to the impeller to have the same geometries at the inlet test sections and to avoid sudden contraction of the inlet flow. The meridional coordinate of the test section is referenced to the tip of the impeller leading edge. It is expressed as the ratio of axial distance from the leading edge tip to the hydraulic diameter of the wetted area between pipe wall and pump shaft (Figure 11). Section 1-1A is chosen as close as possible to the impeller inlet. The first (upper) volute tongue's position is taken as a reference ($\theta = 0°$) for angular coordinates and impeller's rotation direction is taken as positive.

Wall tappings

Equally spaced 12 wall tappings are drilled around the circumference of the test sections, 1-1A, 1-1B and 1-1C, in order to study the inlet flow symmetry (Figure 11). Inlet wall static pressures are measured with a low range variable reluctance type differential pressure transducer by using scanivalves.

All the pressure measurements; wall static, probe total and dynamic pressures, were referenced to the average pressure of the suction head measurement section S, such as: $h\text{-}h_s$, $H\text{-}H_s$.

Flow traverses

Suction flow traverses are performed along the radii of the test sections, at different angular positions. The number of the flow traverse stations of the Group I are 3, 4, 1 for sections 1-1A, 1-1B, 1-1C respectively. Results of Group I pumps indicated that asymmetry is not pronounced in the flow traverses

as strong as the wall pressure measurements. Unless flow traverses are made at each circumferential position of the test sections, which is not physically possible, it does not make that much difference to perform the flow traverses at a limited number of circumferential stations. Therefore, wall pressure measurements are taken as reference measures on the inlet flow asymmetry and then traverse stations are reduced to two at sections 1-1A and 1-1B for Group II pumps of smaller sizes.

Preliminary experiments at VKI, [3], [4], [5] and [16] and the literature survey indicated that the flow has a three-dimensional character in the suction pipe at partial flow rates. Therefore, three-dimensional flow traverses are done with 5-hole probes which give time averaged values.

The directional holes of the probe intercept quite a large amount of dynamic pressure because they are at 45° with the axis of the probe nose. This fact implies a high dynamic pressure correction factor of the order of,

$$\frac{q_{true}}{q_p} = \quad 1.65$$

The utilization range of the probes is selected as the linear response part of the pitch angle response curve,

$$\frac{P_u - P_D}{q_p} = \quad \text{Constant}$$

For these probes, this range is about ± 10°. The correct values of the probe pressures and angles are determined by means of introducing three-dimensional calibration curves, point by point, in the data reduction program, hence velocity components are calculated.

Exit wall tappings

A series of wall tappings are drilled at the shroud side of diffuser part of the volute, around the circumference, at a radius $R/R_2 = 1.044$ and 1.080 for the groups I and II respectively. At these radii, the jet and wake mixing process has largely taken place. The angular positions of the wall tappings are selected by taking into account the double volute design. The impeller-volute matching flow rate is determined from the impeller exit wall tapping readings, where the circumferential exit static pressure distribution has minimum asymmetry.

Exit flow traverses

Impeller exit flow traverses are performed at the same radius as for wall tappings and at four different angular positions. The flow is considered as two-dimensional, hence two-dimensional probes are used. A wedge probe, which has a proper wedge angle and hole position concerning flow separation, is used for two-dimensional traverses across the impeller exit width. In the case of three-dimensional flow at the traverse station, the insensitivity of the probe to the pitch angle was checked by varying the pitch angle during the calibration. Calibrations show that, generally, the static pressure correction coefficient in the range $-8° < \phi < +8°$ and the total pressure in a range $-15° < \phi < +15°$ are not affected by pitch angle (ϕ).

Measurements error

The errors of the measurements (referred to the nominal point readings) are given below:

Rotational speed	± 0.3%
Torque	± 0.5%
Pressure	± 0.5%
Flow rate	± 0.5%
Angle	± 0.5%

The relative accuracy of the inlet flow traverses is made by comparison of the flow rates, measured with venturi and obtained from the integration of the axial velocity component at nominal flow rates. The statistical average error, referred to in the venturi measurements, is 0.5%. This agreement is spoiled when the reverse flow appears in the suction pipe. In fact, probes detect root mean square mass averaged values for absolute velocity. The comparision of the meaurements with the wedge probe and LDV system made at the same exit station shows that the error on probe absolute flow angle (α_2), due to the jet-wake, does not influence the tangential component of the velocity. The error on α_2 is more pronounced on the meridional velocity component. This effect could be expected to be much less in the suction pipe where the turbulence level is lower than at the impeller outlet.

THE IMPELLER MODELS

The impeller models which were investigated can be divided into two groups, each group being derived from a classical industrial pump model. A double volute was used in both cases and the design objective (flow and head) was kept the same within each group.

A new impeller was derived from the classical reference one, after the complete detailed investigation of the flow at all operating points was obtained. The new experimental evidence was at each step taken into account and the design philosophy adapted accordingly.

The two groups of impellers are:

Group I: $N_s = 37.1$; $\phi = 0.12$; $\psi = 0.865$
PUMPS: REF., No. 1, No. 2, No. 3, No. 4

Group II: $N_s = 46$; $\phi = 0.12$; $\psi = 0.90$
PUMPS: No. 5, No. 6, No. 7; No. 5 being REF. for this group.

The blade number has been modified from 5 to 7, the inlet to outlet area ratio or meridional contraction has been changed over a range of 30% and the blade loading distribution over the channel height by 50%, the loading at the tip was changed by 35%. A summary of the modifications with respect to the reference model of the Group I is made in the following table.

IMPELLER NUMBER	1	2	3	4
Blade number	5	6	7	5
Blade chord (tip)	+16%	—	—	+ 5%
Aspect ratio	− 5%	− 5%	−10%	−15%
OUT/IN area	−25%	−10%	−17%	− 4%
TIP/HUB loading	+ 5%	−47%	−20%	−40%
TIP loading	+11%	−12%	−17%	−40%

This wide spectrum for the hydraulic design parameters, related to the detailed blade shape, resulted in impeller views of which some are shown in Figure 9.

The detailed structure of the prerotation and reverse flow, the angular and pressure fluctuations will be discussed using the reference pump model as an example for the probe measurements, No. 5 for the fluctuating angle measurements and No. 2 for the fluctuating pressure measurements. The different measurement techniques have been developed during the program and have not been applied to all pumps of the two

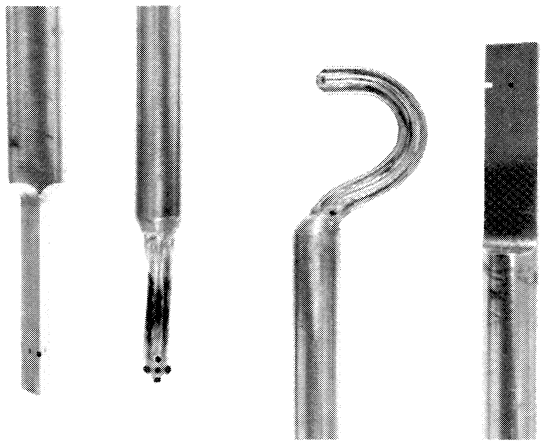

Figure 8. Directional Probes.

groups. It is, however, believed that the phenomena are similar, making abstraction for flow rate and the intensity of the fluctuations at which they occur.

THE OVERALL PERFORMANCE

The overall performance of Group I is summarized in Figure 10 where the design point was identical for all impellers. The nominal point or the experimentally best efficiency point did not coincide with the design point. The scatter within the group is ± 2% on nominal mass flow, ± 1.5% on manometric head and ± 1.5% on overall maximum efficiency. This indicates that a difference in the blade and channel lay-out can result in the same nominal performance. The characteristics at low flow rates are quite different and a remarkable variation in shut-off total head and absorbed power is seen together with a different slope of the H-Q curve. A pronounced influence on the critical flow rate can be expected. The differences at partial flow rate will provide a clear interpretation of the effect of the studied parameters. The increased tip loading and loading distribution produces the highest H-Q curve and highest power at low flow rates (impeller 1).

DETAILED PERFORMANCE

Determination of critical flow rate Q_{cr}

The critical flow rate is determined by flow surveys in three upstream stations (Figure 11). The appearance of preswirl near the outer wall at the measuring station is called the critical flow rate for that station and extrapolation to the impeller inlet, station X = 0, provides the impeller critical flow rate.

During the radial surveys, one determines also the evolution of the boundary for reverse flow. The sudden appearance of reverse flow is well indicated in Figure 12 for the measurements in station 1-1A. These flow explorations with multidirectional probes are performed in other azimuthal positions for the same plane and in the other axial stations.

The results are summarized in Figure 13, where the critical flow rates for the four impellers of Group I are compared. The flow ratio Q_{cr}/Q_N equals 0.70, 0.83, 0.53 and 0.68, while the power ratio P_{cr}/P_N varies as 0.85, 0.94, 0.76 and 0.87 for the reference No. 1, No. 2 and No. 3 impeller. The critical head changed from 0.96 (No. 1) to 1.04 (No. 2 impeller) with respect to the value 1.0 for the reference model.

Similar observations are made for the Group II where

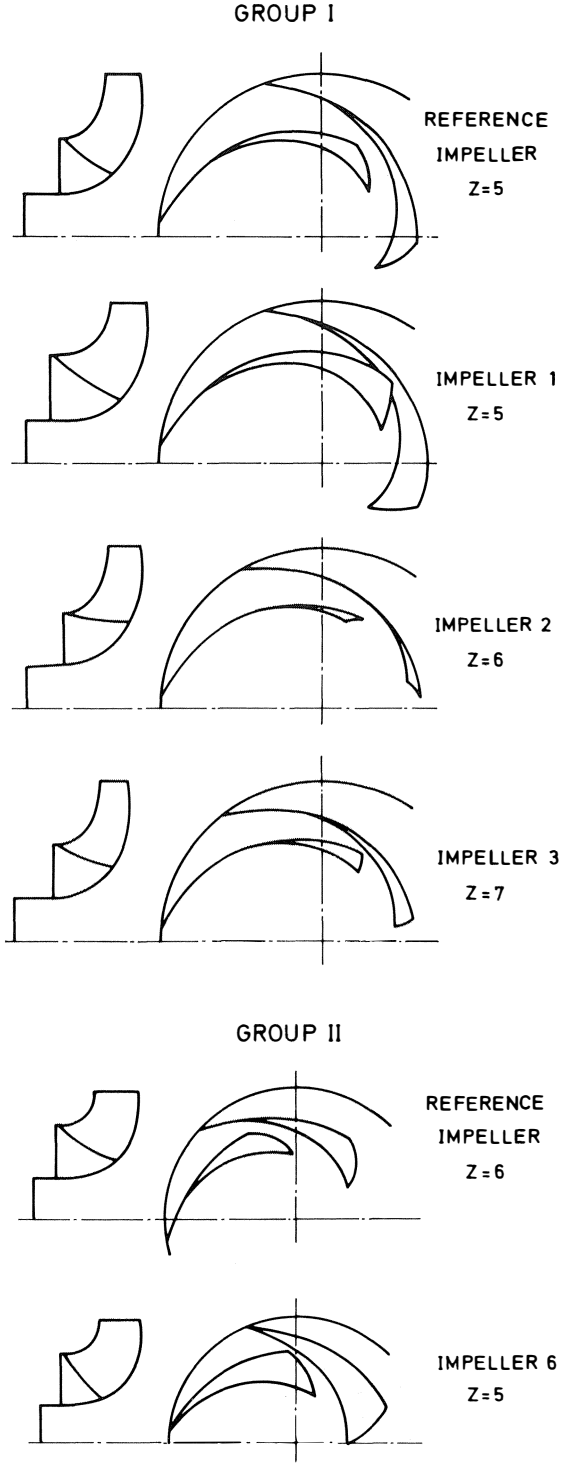

Figure 9. Meridional and Front View of Test Impellers.

Q_{cr}/Q_N is changed from 0.88 to 0.77 at the higher specific speed design.

The inlet flowfield

The appearance of the prerotation causes a complicated three-dimensional field at the inlet plane of the pump, a description of which can be obtained from the wall pressures

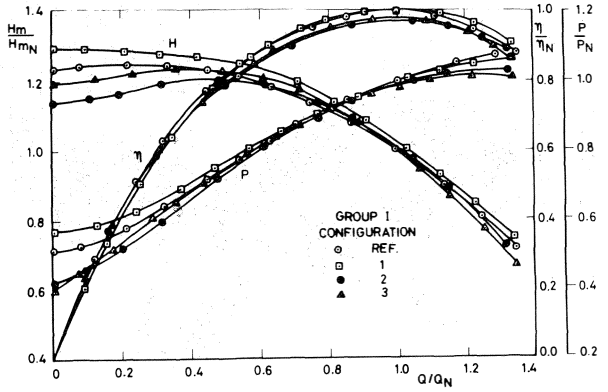

Figure 10. Performance Characteristics of the Group I Pumps.

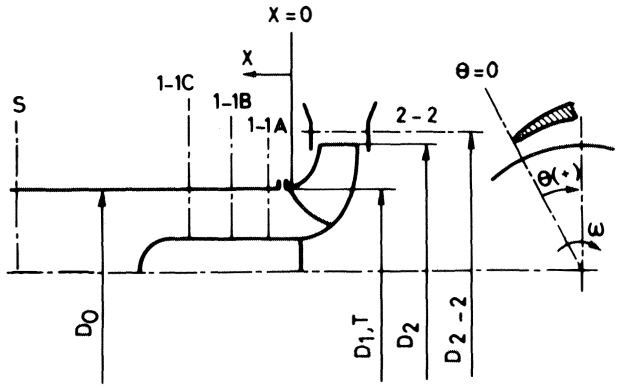

Figure 11. Inlet Sections for Detailed Flow Traverses.

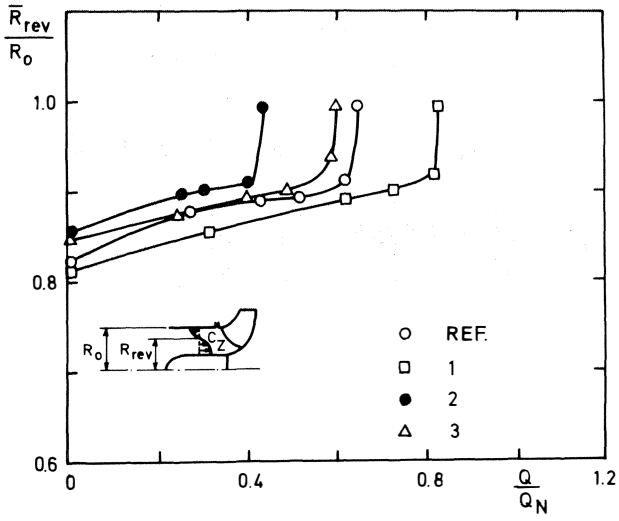

Figure 12. Radial Extension of Reverse Flow.

and probe measurements. Time averaged values are only observed in this part of the investigation and the local values are measured with respect to the suction inlet static pressure

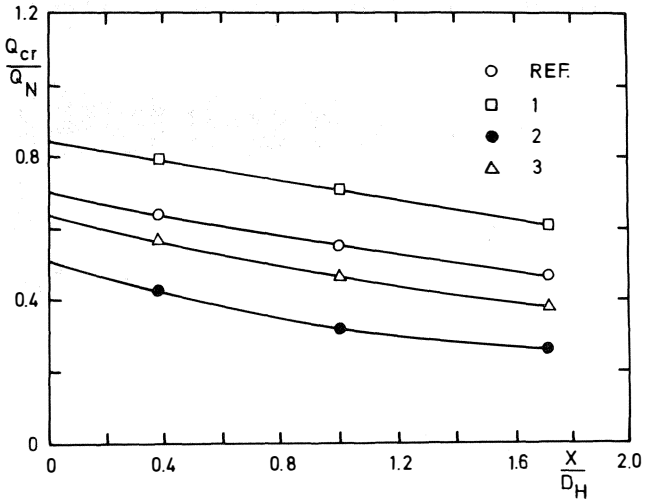

Figure 13. Critical Flow Rate Determination.

and non-dimensionalized by dividing through the impeller inlet tip speed

$$\triangle H_{(w)} = \frac{h_{(w)} - h_s}{U_{1,T}^2/2g}$$

$$\triangle H_0 = \frac{H_0 - h_s}{U_{1,T}^2/2g}$$

$$V_z = \frac{V_z}{U_{1,T}}$$

$$V_\theta = \frac{V_\theta}{U_{1,T}}$$

$$V_R = \frac{V_R}{U_{1,T}} \; ; \quad V'_R = \frac{V'_R}{U_2}$$

All measurements in the inlet plane nearest to the impeller are discussed for the flow range $Q_n \rightarrow$ zero flow.

The phenomena are now discussed using the reference impeller as an example, with all models showing the same features at different absolute values of the flow rate. The inlet wall static pressure is observed from 0° → 360° during the throttling process from 122% $Q_N \rightarrow$ 5% Q_N. Good circumferential uniformity is observed as long as Q_{cr} is not arrived at. The development of prerotation increases the wall pressure to 25% of $U_{1,T}^2/2g$ value, which decreases as one proceeds further upstream in the inlet duct. A non-uniformity is observed and probably must be linked to the azimuthal position of the volute tongues. A strong non-axisymmetry is observed in the impeller outlet plane during the operation in the prerotation zone; this was connected to the position of the tongue for each volute. The designs with the lower Q_{cr} (0.53 Q_N instead of 0.70 Q_N) do show a better uniformity and a maximum $\triangle H_w$ coefficient of ⅓

of this value. The correlation between Q, Q_{cr} and the wall pressure coefficient, $\triangle H_w$, averaged over 360°, is shown in Figure 14 for four different designs.

The detailed flow exploration over the inlet channel height in the same inlet plane is shown for four flow rates; Q = 1.02, 0.61, 0.43 and 0.0 Q_N. Constant inlet flow conditions are observed for the nominal flow rate. The static and total pressure coefficient are gradually shifting to large values when prerotation establishes itself in the plane of observation. The total pressure coefficient reaches a value of 100% near the outer radius in the inlet duct in Figure 15. The fluid is receiving more and more energy from rotating impeller motion through the return flow and the entrainment effect spreads over the inlet duct. The area averaged total energy for the suction flow is characterized by $\triangle H_0$ and Figure 16 shows clearly the relation between low Q_{Cr} and low $\triangle H_0$ to be dissipated in the suction pipe. The solid body rotation of the fluid, as shown in the next paragraph, causes the large energy input at the outer radius.

The velocity V and the non-dimensionalized velocity components V_z, V_θ and V_R are summarized in Figures 17 and 18. The prerotation suppresses the axial component at the outer radius as V_z approaches zero and becomes negative: the

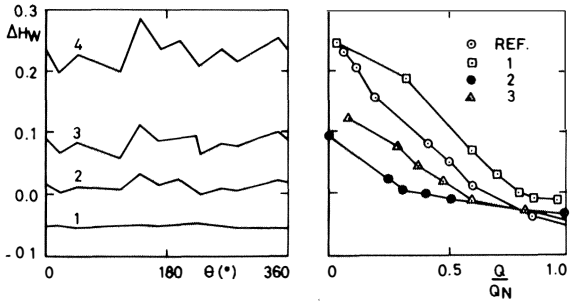

Figure 14. Inlet Flow Asymmetry — Wall Static Pressure — Reference Pump — Plane 1-1A.

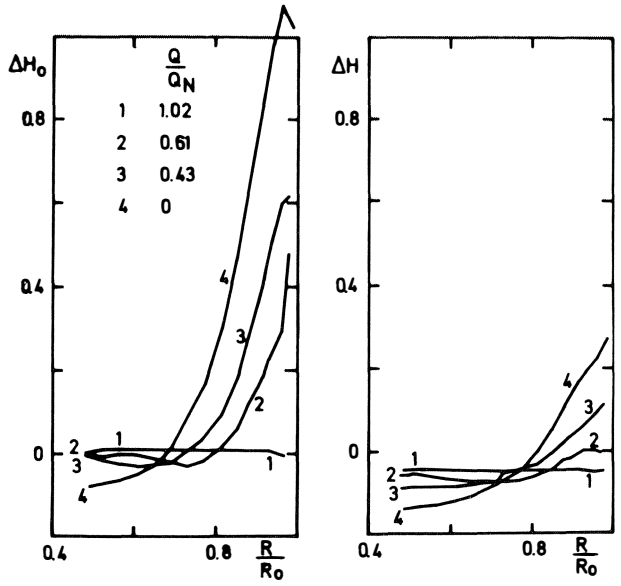

Figure 15. Total and Static Head Evolution — Reference Pump — Plane 1-1A.

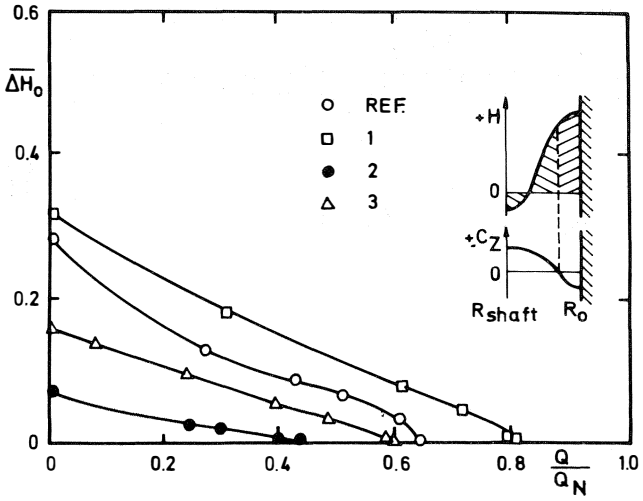

Figure 16. Integrated Total Inlet Head — Reference Pump — Plane 1-1A.

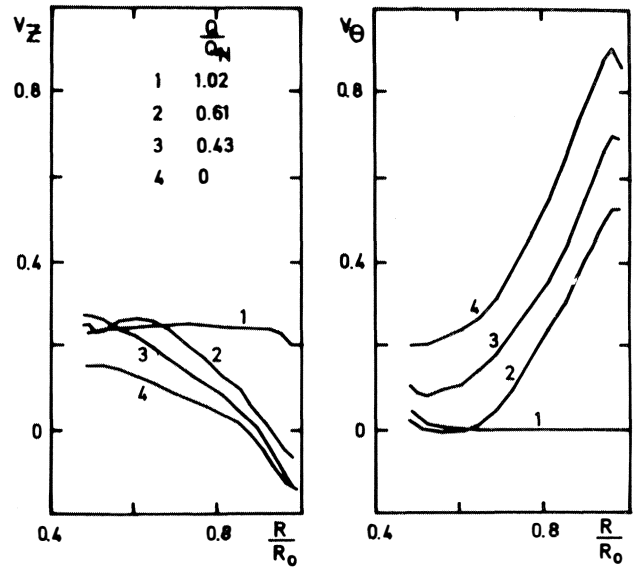

Figure 17. Evolution of Axial and Tangential Velocity — Reference Pump— Plane 1-1A.

return flow crosses the measuring plane and the inlet flow angle is past 90° (tangential). The tangential component, V_θ, non existant at Q_n, increases and tends towards 1.0: the fluid is entrained by the impeller at impeller speed and has a very small axial component. The fluid behaves partly as a solid body in rotation. The radial component, V_R, is slightly negative at Q_N: it means a small radially outward component. These measurements are performed near the impeller inlet face and the radial motion of the streamline in the meridional plane is already detected. The return flow causes an opposite effect since the fluid comes down, out of the impeller, and a positive angle of 8° is measured, based on V_R and V_θ since $V_z = 0$. The prerotation is a helicoidal motion with a strong tangential velocity component, a small upstream axial and an inward radial component. Fluid is entrained by the flow which returns from the rotating impeller and the motion attenuates in the upstream duct. Energy is added to the arriving fluid and has to

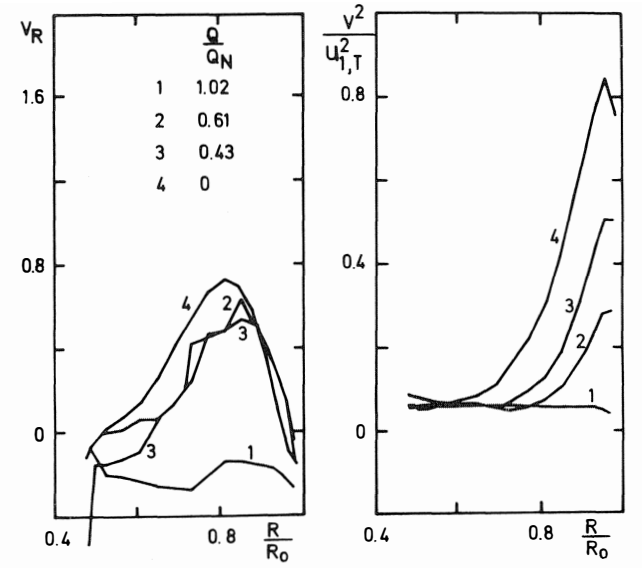

Figure 18. Evolution of Radial and Total Velocity — Reference Pump — Plane 1-1A.

be dissipated. At a given cross section, an inner core flows toward the impeller, while in the outer ring, the return fluid circulates.

The impeller outlet flow field has been studied using the same approach as for the inlet duct study. One illustration of the problems in the outlet section during the occurrence of prerotation is given in Figure 19. The velocity in the meridional plane V'_R approaches zero near the inner and outer walls for Q_N. The region of the blade width over which "negative" velocities occur increases with throttling until a total collapse is observed at the smallest flow rate. Zero velocities are seen at the extremities and the central part is totally suppressed. These results do suggest that important recirculating flows occur in the rotating channels.

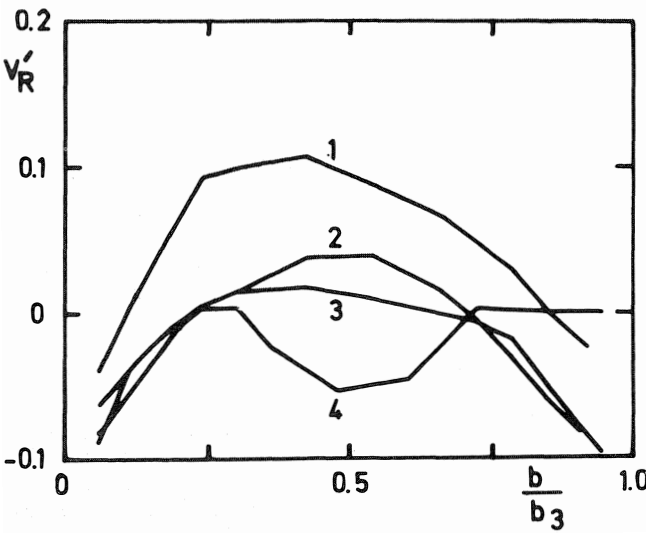

Figure 19. Impeller Exit Meridional Velocity — Reference Pump.

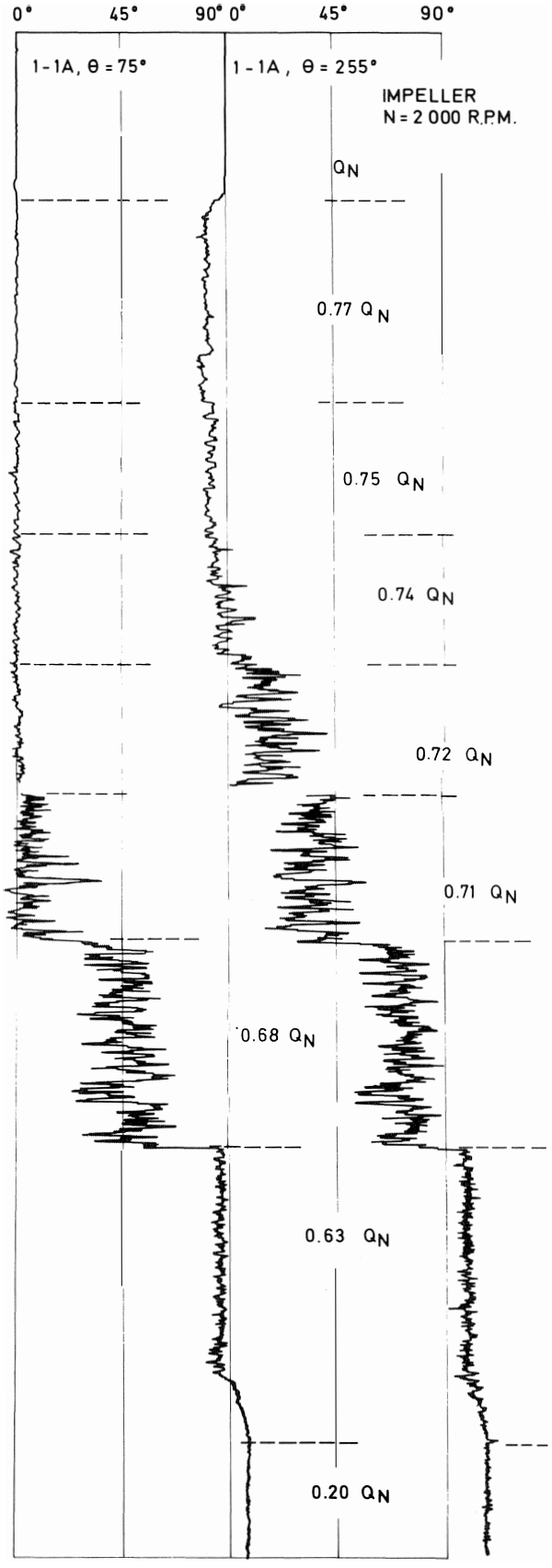

Figure 20. Evolution of Inlet Angle with Flow Rate — Pump No. 5 — Plane 1-1A.

DETAILED PERFORMANCE — UNSTEADY MEASUREMENTS

Preliminary experiments carried out with a transparent plexiglas suction pipe demonstrated the existence of a highly unsteady inlet flow at partial flow rates. Therefore, besides the time averaged measurements, some unsteady flow measurements are performed at the suction pipe and at the exit of the impeller. Time-dependent static pressure measurements on the suction pipe wall and on the volute diffusing part front shroud wall were taken with fast response piezoelectric pressure transducers. Spectral analysis of both the inlet and exit wall pressure signals were taken simultaneously by means of PDP data processing system in order to find the dominating frequency of the pulsating flow. Time-dependent yaw angle measurements in the suction pipe were taken with vane-potentiometer systems at different axial and angular test stations. A rectangular shaped, thin and flat vane, is fixed to the shaft of a potentiometer. The vane's height is determined in such a way that the vane would always remain in the reverse flow region which is obtained from the radial flow traverses made by the 5-hole probes. Sealing of the system from the water is provided with leak-proof ball bearings which have very low friction. Measurements were taken at two different angular positions at the same section to see if the unsteady flow has a propagating character, similar to rotating stall.

Flow angle measurements

Two small rectangular vanes have been installed, 180° apart, near the outer radius of the inlet suction pipe. The angular flow variations in this region have been recorded for the complete pump characteristic. The two tangential stations are 75° and 255° with respect to the volute tongue and the measuring plane, 1-1A, is closest to the impeller inlet face. A continuous record has been made for different pumps and the reference impeller of Group II is chosen as the example in Figure 20. The flow is perfectly axial and steady at the Q_N flow rate. A counter-rotation of 75°, slightly fluctuating, is observed in one circumferential station at 0.77 Q_N to 0.74 Q_N flow range. Based on the results at the station $\theta = 255°$ one would conclude that $Q_{cr} = 0.73\ Q_N$ when the observations at $\theta = 75°$ indicate $Q_{cr} = 0.71. \ . \ .0.70\ Q_N$ which corresponds to the probe results. A few per cent discrepancy can exist between different circumferential stations. The counter rotation swirl, before the flow rate equals Q_{cr}, is observed in one position. This type of flow was postulated by Stepanoff at flow rates higher than Q_N, which is not our case. The large fluctuations in the small region of $Q = 0.72$ to $0.68\ Q_N$ are clearly shown. At $0.63\ Q_N$, the inlet flow at the measuring station became tangential and the angular fluctuations are strongly diminished. Further throttling provides the reversed flow at the section 1-1A of the inlet suction pipe.

The average inlet flow angle and the fluctuations are related to the particular operating point in a pump performance map as shown in Figure 21.

The prerotation phenomenon and the corresponding angular flow fluctuations are concentrated in a small flow range, points 3 → 10 in Figure 21. During this sequence, the average

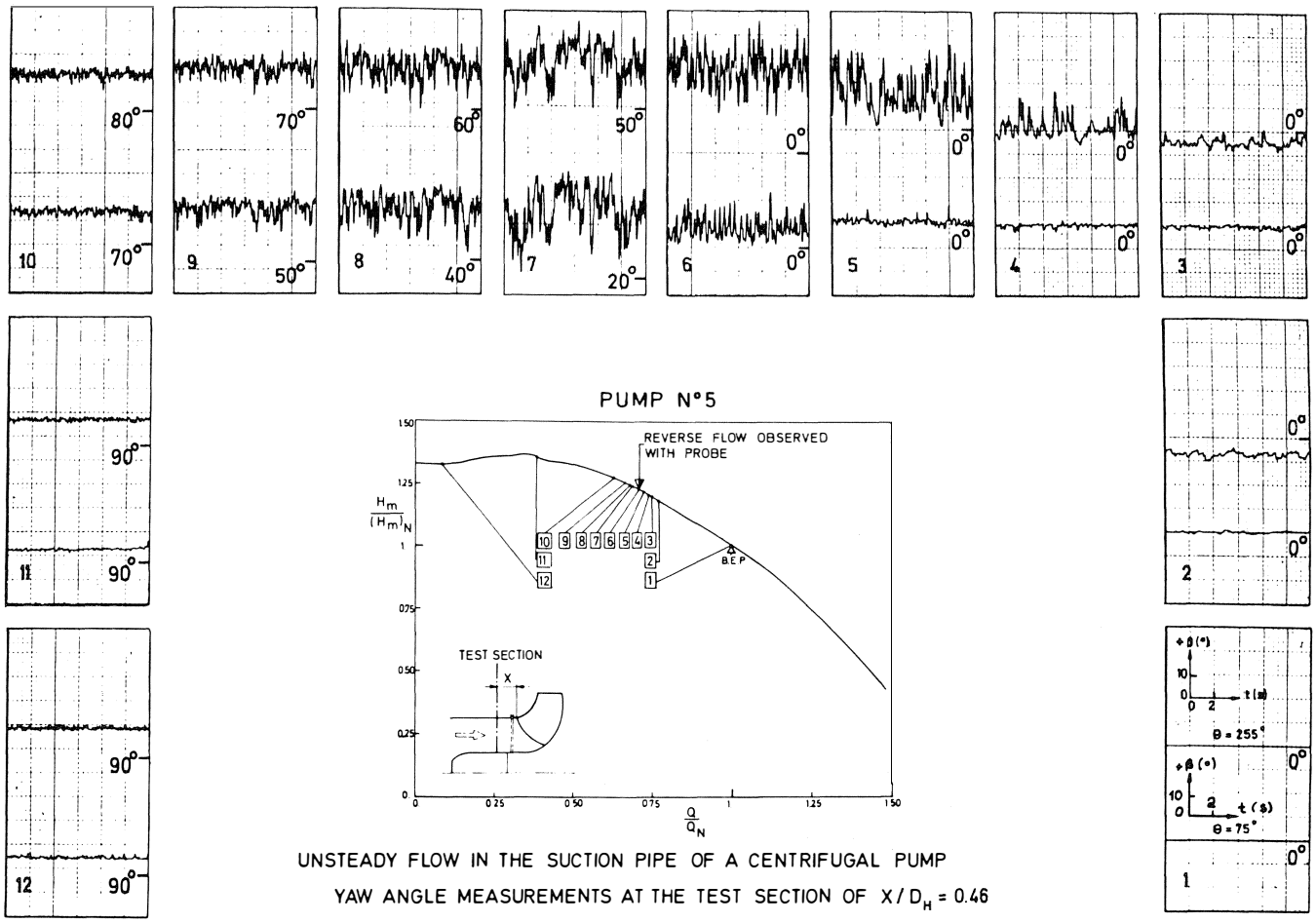

Figure 21. Performance Map and Inlet Angle Evolution — Pump No. 5.

inlet flow direction changes from axial (0°) to tangential (90°). Further throttling, points 10 → 12, increases the average flow angle from 90 ° to 105°. A steady return flow is established at the outer annulus of the inlet duct. The peak to peak maximum fluctuations amount to 30% and occur at an average inlet flow angle of 50° to 60° from the axial direction. The frequency of the fluctuating flow seems to be 30% of the impeller frequency once prerotation has developed, as shown in Figure 22. The mean angles found by the vane check very well with the probe results as shown in Figure 23.

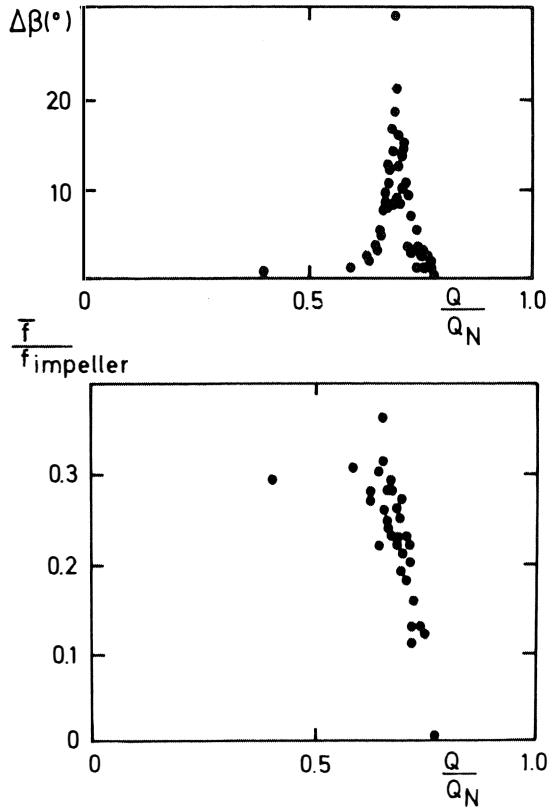

Figure 22. Amplitude and Frequency of the Fluctuating Angles — Pump No. 5.

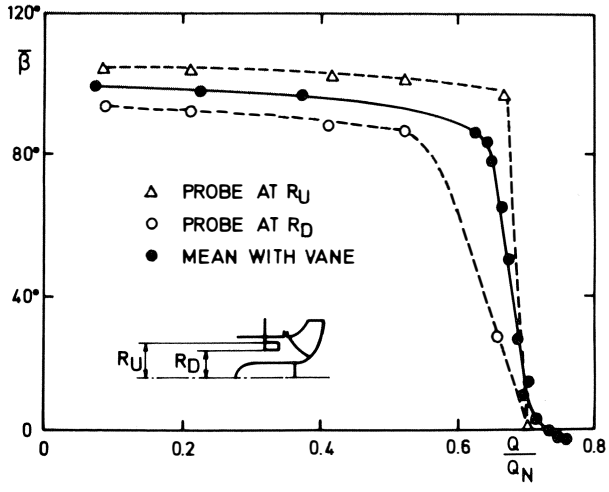

Figure 23. Comparison of Probe and Vane Results — Pump No. 5.

The starting of the reverse flow and prerotation has an unsteady character. The unsteadiness appears within a very small flow rate range around Q_{cr}. The spectral analysis of the angular fluctuations is performed on the recorded data (sampling rate 1384 Hz) for the flow rate Q = 0.717, 0.700, 0.680, 0.647, 0.447 and 1.00 Q_N. The results are shown as a log (β^2) versus log (freq.) in Figure 24. The blade passing and its harmonics are the dominating frequencies at the nominal flow rate. At the occurrence of the prerotation, the power spectra for the inlet flow angle change drastically. The low frequency contribution is increased by three orders of magnitude and the dominating frquencies are 27 Hz and 44 Hz with the harmonics at Q = 0.717 Q_N. The content at the low frequency range is further increased by two orders of magnitude at Q = 0.700 Q_N and the harmonics have disappeared. The large flow fluctuations have only a low frequency content. This evolution is continued for Q = 0.680 Q_N. At this flow rate, the largest angular deviations were observed at θ = 75° in Figure 20. Further throttling decreases the contribution of the low frequencies in the power spectra and a slight shift towards higher frequencies is observed at Q = 0.44 Q_N. The low frequencies contribution will further diminish towards the shut-off conditions.

These measurements have been performed on two other pump models where similar phenomena were observed. The data are not sufficient in order to make firm conclusions on the relation between the maximum fluctuations of the inlet flow angle, the frequency of the prerotation phenomena and the design, parameters of the impellers. The frequency of the prerotation (from the angle variations) has been observed to be 30% and 15% of the impeller rotation for two different models.

Unsteady pressure measurements

The unsteady wall pressure measurements were performed using a piezoelectric crystal, flush mounted in the instrumentation ports previously used for the flow traverses. A 5 psi transducer is used for the inlet plane and a 75 psi transducer in the outlet plane of the impeller. The calibration of the measuring chain is performed by exposing the transducers to a known pressure pulse.

Examples of some inlet wall pressure fluctuations are shown in Figure 25. The results are from impeller No. 2 at 1300 RPM, the pressure traces and the time for the impeller revolutions are shown. Three operating conditions have been chosen; namely Q = Q_N, 0.10 Q_N and Q_{cr}. The blade-to-blade pulsations for this 6 bladed impeller are clearly observed at nominal and near shut-off conditions. The unsteady swirling flow which starts at Q_{cr} produces a pressure signal which is superposed on the blade-to-blade trace measured in the inlet plane 1-1A.

The following conclusions can be made from the observations on three impeller models:

- blade passing frequency is present in the unsteady pressure signal for all flow rates.
- the peak to peak fluctuations, at blade passing frequency, grow from Q_{MAX} toward Q_{cr} and seem to decrease during the throttling from Q_{cr} to shut-off.
- blade-to-blade pressure fluctuations at shut-off increase proportionally with the peripheral velocity signal. Therefore a pressure coefficient C_p is defined for the nondimensional representation which takes this into account.

The blade-to-blade pressure fluctuations at Q_{NOM} do vary from design to design with a factor of 5/1. This variation can be

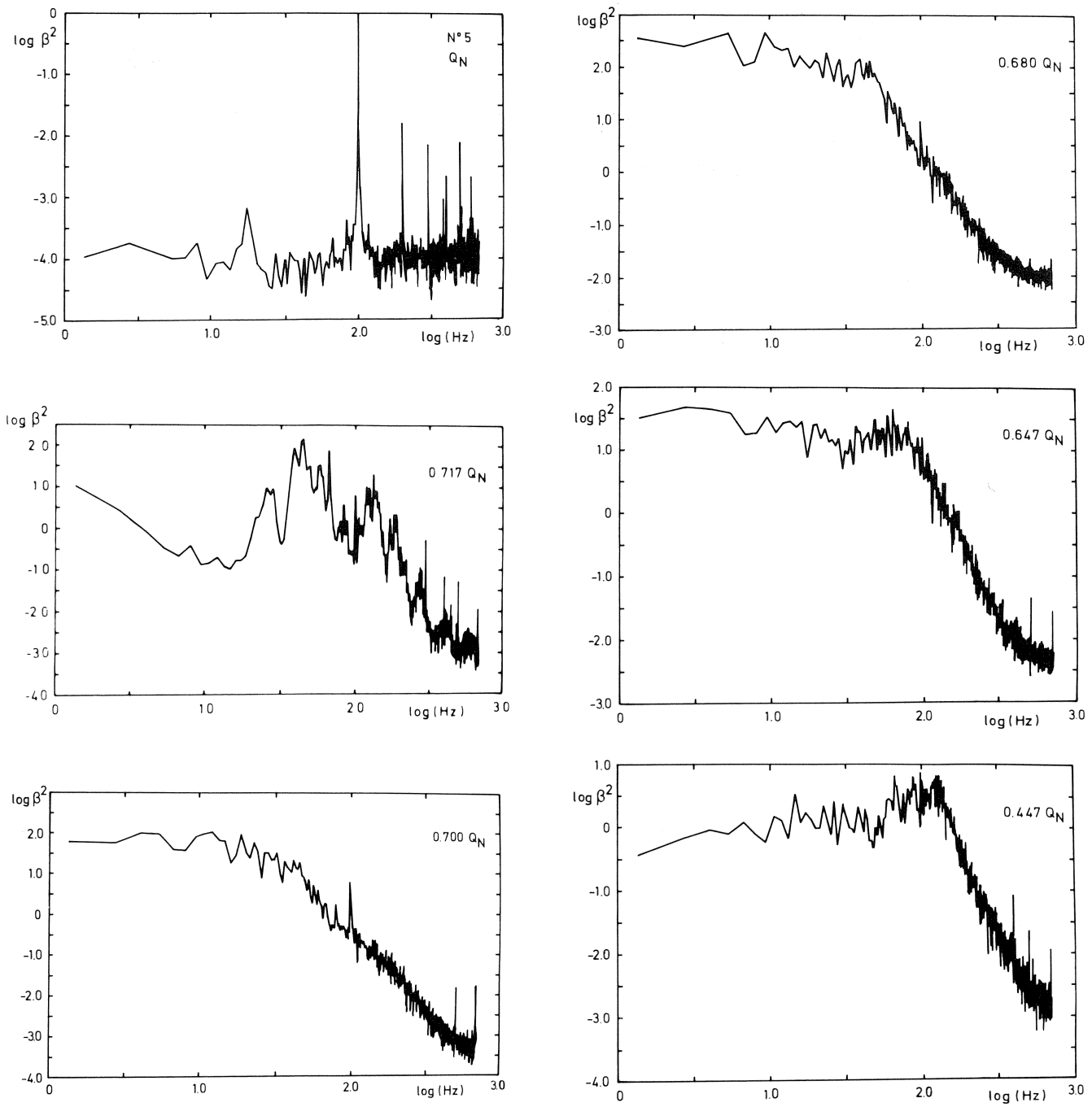

Figure 24. Power Spectra of the Angle Variations — Pump No. 5.

traced down to be a result from the difference in tip-to-hub blade loading. The higher the radial distribution of the loading, the larger the pressure pulses will be. A loading variation of tip/hub = 2.37, compared to 1.32, gave the above mentioned results.

The larger pressure pulses in the inlet field at Q_{NOM} are an indication for the critical flow condition at the tip and the critical flow rate is observed to be 0.83 Q_N. Once Q_{cr} is obtained, an additional pulsation occurs at a much lower frequency, namely 30% (impeller No. 2) to 50% (impeller No. 1) of the rotational frequency.

The pressure coefficient C_p shows the following evolution for two extreme cases from which fluctuating wall pressures were obtained.

C_p	Model N° 1	Model N° 7	Type
Q_{MAX}	1.2%		Blade
Q_{NOM}	2.6%	0.13%	passing
Q_{cr}	5.2%	—	frequency
$Q=0$	2.5%	1.3 %	
Q_{cr}	6.3%	—	frequency of
$Q=0$	5.0%	—	swirling flow

The signals from the wall pressure measurements on the No. 5 impeller were analyzed using a Fast Fourier transform technique. The results, log p^2 as a function of the frequency,

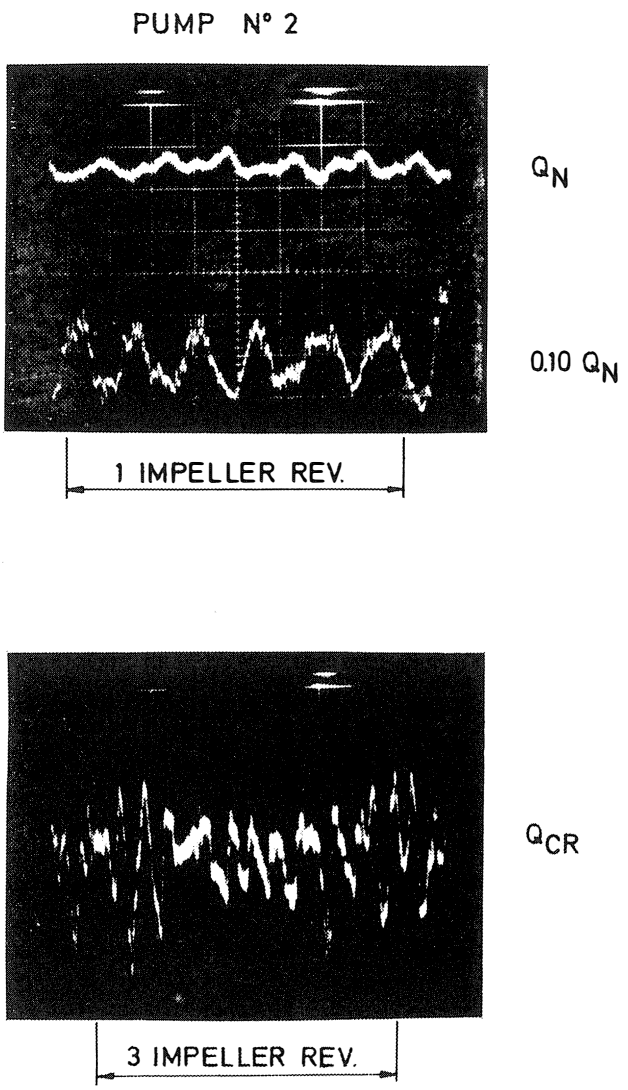

Figure 25. Fluctuating Wall Pressures — Pump No. 2 — Plane 1-1A.

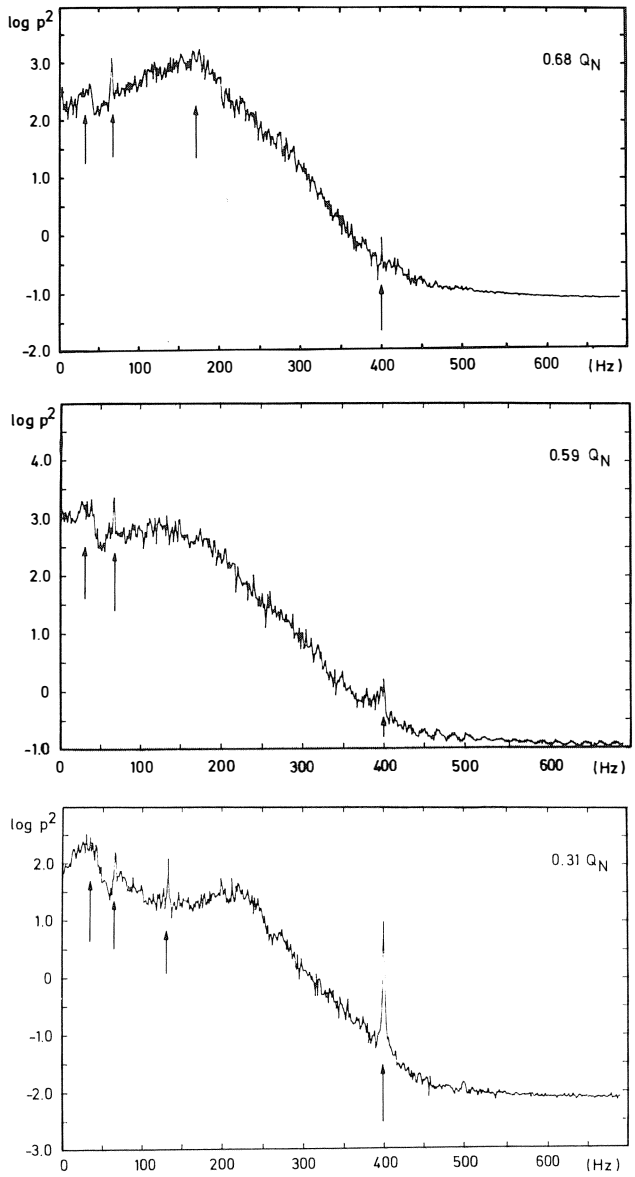

Figure 26. Power Spectra of the Fluctuating Pressures — Pump No. 5 — Plane 1-1A.

are shown for the mass flows 0.68 Q_N, 0.59 Q_N and 0.31 Q_N. The prerotation is well developed at its maximum for the fluctuating components (0.68 Q_N) and transforms into the reverse flow (0.31 Q_N). The once and twice per revolution signal, with the blade passing frequency, are observed. The shift in the power spectra content from blade passing frequency (at 0.68 Q_N) to the lower frequencies is observed (at 0.31 Q_N). The perturbation frequency is difficult to determine from this representation and the 133 Hz and 400 Hz signal have not been explained yet. This analysis illustrates that once past Q_{cr}, the low frequency perturbation at sub-impeller frequency, starts contributing more and gradually takes over from the events at blade passing frequency. The physical explanation could be that the flow is first stalled in each channel with relatively small mass involved, then a reorganization takes place and a much larger mass flow is entrained at lower frequencies (Figure 26).

CORRELATION OF RESULTS

The analysis of the overall performance and the detailed flow situations occurring at all operating conditions of the different pumps led to a set of conclusions concerning the phenomena at partial flow rate.

The pump total head at partial flow rates and the critical flow rate Q_{cr} are closely related to each other due to the fact that both are controlled by the same mechanism. This mechanism is the relative flow diffusion. Although all impellers in one group had the same nominal performance, differences were present in the way this was obtained. Impellers having high diffusion rates (DR) at the nominal point, have also a higher Q_{cr} and a higher total head than those having lower diffusion rates.

The relative velocity diffusion (RVD) is the dominant flow factor affecting the starting of prerotation and reverse flow. A high RVD at the tip section will cause early stalling of the impeller flow and hence a high critical flow rate. The analysis showed that none of the design parameters, considered individually, control the pump critical flow rate alone. All the parameters, mentioned in the paragraphs on the model definition and overall performance, are combined in a pump parame-

ter PP, and the Q_{cr} flow rates are correlated with respect to the reference impeller. The result is shown in Figure 27.

This remarkable correlation was encouraging to further refine the definition of the diffusion process in a pump impeller and achieve an average error between predicted and actual Q_{cr} of 3.8% using the design information in the prediction scheme.

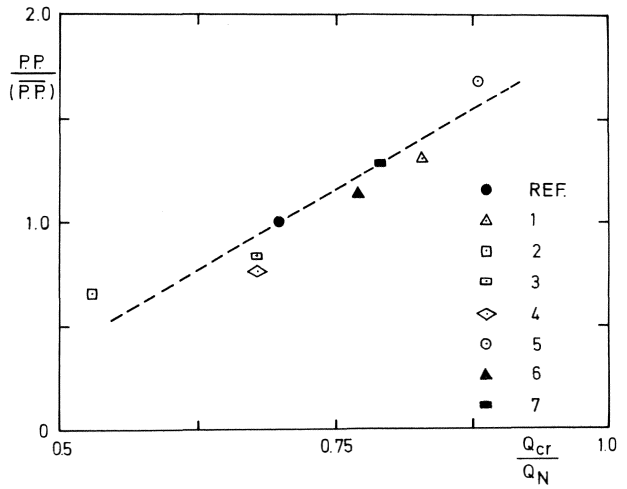

Figure 27. Critical Flow — Pump Parameter Correlation.

CONCLUSION

This systematic investigation involved the determination of the source of the reverse flow and prerotation, i.e., the impeller itself. The part of the pump impeller where flow separation is most likely to occur is the impeller shroud wall joint line on the suction side of the blades. This separation, when it develops, will cause the inlet flow perturbations.

The design parameters, such as loading and loading distribution, do influence the flow separation and therefore the critical flow rates as have been shown. The pump Q_{cr} depends on the impeller design.

The reverse flow carries a high amount of energy which is produced by the impeller and has to be dissipated in the suction pipe. The pump head instability, or positive slope of the H-Q curve, at partial flow rates is not related to the intensity of the reverse flow. The reduced reverse flow design has also a reduced pump shaft power at partial flow rates and shut-off conditions.

The transition from the appearance of prerotation to a reverse flow condition occurs over a small flow range. The flow tends towards a solid body rotation in the suction pipe. The angular and pressure perturbations are maximum in the small range where the transition from axial to tangential flow at the outer radius takes place. The energetic content of the fluctuating components shifts from blade passing to sub impeller rotational frequency during the transition, whereafter the low frequency content diminishes again. The sub impeller frequency is similar to a rotating stall cell phenomenon in compressors. Near shut-off, a continuous reverse flow seems to be established near the outer part over 360 ° of the circumference of the suction pipe.

The detailed design parameters could be correlated and a pump parameter combining the investigated features could be formed, helping in an effort to predict Q_{cr} from design inputs.

A basis for further correlation between the fundamental flow phenomena and mechanical and acoustical effects is provided. The similarity aspect of prerotation and reverse flow has to be confirmed over a large range of operations and the non-dimensionalized parameters, the fluctuating pressures and flow angles have to be related to more general and easier measured parameters for factory and field use.

ACKNOWLEDGEMENTS

The authors acknowledge gratefully the support of the Worthington SPA Company of Italy, which provided the different pump models and sponsored the major part of this effort.

REFERENCES

1. Fraser, W. H.: Flow recirculation in centrifugal pumps. 10th Annual Turbomachinery Symposium, Dec. 1-3, 1981.
2. Morton, T. & Olin, G. L.: Realistic design specifications increase pump reliability. 10th Annual Turbomachinery Symposium, Dec. 1-3, 1981.
3. Ferrini, F.: Some aspects of self-induced prerotation in the suction pipe of centrifugal pumps. Worthington European Technical Award, Vol. III, 1974.
4. Schiavello, B.: Optimization of pump design based on a parametric study. VKI PR 1975-14.
5. Sen, M.: Experimental study on the inlet flow field of a centrifugal pump. VKI PR 1976-12.
6. Stepanoff, A. J.: Centrifugal and axial flow pumps. 2nd Edition, Chapter 3, 1957.
7. Peck, J. F.: Investigation concerning flow conditions in a centrifugal pump, and the effect of blade loading on head slip. Proc. Inst. Mech. Engrs., Vol. 164, 1951, p 1.
8. Schweiger, F.: Flow in centrifugal pumps working at part capacity. NEL Report No. 245, 1966.
9. Murakami, M. & Heya, N.: Swirling flow in suction pipe of centrifugal pumps — 1st Report: Distribution of velocity and energy. Bull. JSME, Vol. 9, No. 34, 1966, p 328.
10. Lewthwaite, J. C. & Worster, R. C.: Note on the effect on pump stability of guide vanes. BHRA TN 789, 1963.
11. Schmiedl, E.: Untersuchungen an einer halbaxialen Spiralgehausepumpe mit Laufrädern verschiedener Schaufelzahl und Austrittswinkel. Ph.D. Thesis, Tech. Universitat Carolo-Wilhelmina zu Braunschweig, 1971.
12. Dufays, M.: The effect of volute and throttling of the inlet area on prerotation in centrifugal pumps. VKI PR 1977-10.
13. Worster. R. C.: An investigation of the flow in centrifugal pumps at low deliveries. BHRA RR 770, 1963.
14. Schweiger, F.: Stability of the centrifugal pump characteristics at part capacity. Int. Conf. on Design and Operation of Pumps and Turbines, National Engineering Laboratory, Glasgow, Vol. 1, Paper 3-3, 1976.
15. Sen, M.: Prerotation in centrifugal pumps. in: Off-Design Performance of Pumps, VKI LS 1978-3.
16. Schiavello, B. & Sen, M.: Experimental investigation of centrifugal pump design criteria for minimum reverse flow delivery. Paper presented at Worthington European Technical Award, 1979.
17. Schiavello, B. & Sen, M.: On the prediction of reverse flow onset at the centrifugal pump inlet. Paper presented at the ASME 25th Annual International Gas Turbine Conference, 1980.

18. Sen, M.: Study of inlet flow of centrifugal pumps at partial flow rates. Ph.D. Thesis, University of Brussels, June 1980.

NOMENCLATURE

A area

C_p $\dfrac{\Delta P_w}{U_{2,R}^2/2g}$ pressure coefficient for the fluctuating pressures

D diameter, discharge section

DR diffusion ratio ($w_{1,T}/w_2$)

g gravity constant (9.802 m/sec^2)

H total head (m)

h static head (m)

N RPM

N_s specific speed

P pressure

P power

Q mass flow rate

q dynamic head

R radius

RVD relative velocity diffusion $\dfrac{w_1^2 - w_2^2}{2g}$

SN_s suction specific speed

U peripheral speed

V velocity; volume flow rate [m^3/sec]

$V_{z,\theta,R}$ non-dimensionalized velocity components $\dfrac{V_{z,\theta,R}}{U_{1,T}}$

V_R' non-dimensionalized impeller exit meridional velocity component

w relative velocity

α absolute flow angle

β relative flow angle

γ specific weight

ΔH static pressure coefficient $\Delta H = \dfrac{h - h_s}{U_{1,T}^2/2g}$

ΔH_w wall static pressure coefficient

ΔH_o total pressure coefficient

ΔP_w peak to peak pressure fluctuation

χ axial distance

θ azimuthal coordinate = 0° position of volute tongue

ϕ pitch angle

Φ flow coefficient V_{m2}/U_2

ψ head coefficient $\dfrac{H}{U_2^2/2g}$

Subscripts

0 impeller eye, total conditions

1 impeller leading edge

2 impeller trailing edge

cr critical

D down (for probes, discharge suction)

N nominal

MAX maximum

m meridional

H hub

p probe

R radial

s suction section

T tip

u up (for probes)

z axial

w wall

θ tangential

$N_s = \dfrac{N.V^{1/2}}{H^{3/4}}$

$SN_s = \dfrac{N.V^{1/2}}{H_s^{3/4}}$

$H_s = \dfrac{P_0 - P_{VAPOR}}{\gamma}$

N RPM

V = volume flow [m^3/sec]

H head [m]